# Nanoparticle Transport in Epithelial Cells: Pathway Switching Through Bioconjugation

*Robyn Fowler, Driton Vllasaliu, Francisco Fernández Trillo, Martin Garnett, Cameron Alexander, Helen Horsley, Bryan Smith, Ian Whitcombe, Mike Eaton, and Snow Stolnik**

*The understanding and control of nanoparticle transport into and through cellular compartments is central to biomedical applications of nanotechnology. Here, it is shown that the transport pathway of 50 nm polystyrene nanoparticles decorated with vitamin $B_{12}$ in epithelial cells is different compared to both soluble $B_{12}$ ligand and unmodified nanoparticles, and this is not attributable to $B_{12}$ recognition alone. Importantly, the study indicates that vitamin $B_{12}$-conjugated nanoparticles circumnavigate the lysosomal compartment, the destination of soluble vitamin $B_{12}$ ligand. Whereas cellular trafficking of soluble $B_{12}$ is confirmed to occur via the clathrin-mediated pathway, transport of $B_{12}$-conjugated nanoparticles appears to predominantly take place by a route that is perturbed by caveolae-specific inhibitors. This data suggests that, following its conjugation to nanoparticles, in addition to dramatically increasing the cellular uptake of nanoparticles, the normal cell trafficking of $B_{12}$ is switched to an alternative pathway, omitting the lysosomal stage: a result with important implications for oral delivery of nanoparticulate diagnostics and therapeutics.*

## 1. Introduction

Synthetic drug carriers that exploit natural cellular transport pathways are highly desirable for diagnostic and therapeutic applications.[1,2] Of particular interest are carriers that resemble viruses and their ability to target and be internalized by cells, but which are not infective or toxic. Features of viruses important in their cellular trafficking are their size (50–150 nm range) and their functional surface ligands, especially for cellular and sub-cellular receptors. It is not surprising therefore that many synthetic drug delivery systems have been based on virus-inspired designs.[3,4] These typically involve a therapeutic compound incorporated into a nanoscale carrier 'core', which is coated with ligand(s) aimed to specifically guide the carrier towards a particular cellular pathway, enabling delivery of the incorporated therapeutic to a desired location.[5] However, the carrier may not adopt the assumed ligand-directed pathway, as demonstrated by a recent landmark paper,[6] which indicated that some trafficking pathways can be perturbed by synthetic nanoparticles in ways that differ from the transport activated by the viral or bacterial ligand functionality alone.

Here we set out to probe if a ligand-mediated pathway, well-characterized for transport of molecules into and through the epithelial cells of the gut, could be exploited by model nanoparticle drug carriers for potential systemic delivery of biotherapeutics via mucosal surfaces. As the bioconjugate ligand we selected vitamin $B_{12}$, as its intestinal

R. Fowler, Dr. D. Vllasaliu, Dr. F. F. Trillo, Dr. M. Garnett, Prof. C. Alexander, Dr. S. Stolnik
School of Pharmacy
University of Nottingham
University Park, Nottingham, NG7 2RD, UK
E-mail: snow.stolnik@nottingham.ac.uk
Dr. H. Horsley, Dr. B. Smith, I. Whitcombe
UCB, 216 Bath Road, Slough, Berkshire, SLN 4EN, UK
Prof. M. Eaton
ETP Nanomedicine,
c/o VDI/VDE Innovation + Technik GmbH, Steinplatz 1, 10623 Berlin, Germany

DOI: 10.1002/smll.201202623

NANO MICRO small

uptake has already been considered for oral delivery of biotherapeutics.[7–10] Although previous attempts to deliver biotherapeutics directly conjugated to vitamin $B_{12}$ have resulted in loss of therapeutic activity due to digestion of the labile biotherapeutic in the gastrointestinal tract,[11,12] more recent studies have evaluated vitamin $B_{12}$-conjugated nanoparticulates as carriers with the potential to incorporate and protect the biotherapeutic.[10,13]

Importantly however, the use of $B_{12}$-conjugated nanocarriers to deliver biotherapeutics across the intestinal surface assumes that the $B_{12}$-nanoparticles traverse the epithelium in a manner that follows the soluble vitamin $B_{12}$ pathway, i.e. the attached nanoparticle does not perturb the biological transport pathway. This would involve cellular internalization of the entire cubilin receptor-intrinsic factor-$B_{12}$-nanoparticle complex bound to megalin receptor via clathrin-coated vesicles,[14,15] followed by an endosomal stage where the cubilin and megalin receptors dissociate from the complex and recycle to the epithelial cell surface. The remaining intrinsic factor (IF)-$B_{12}$-nanoparticle complex would then be transported to the lysosome (where, in the case of soluble $B_{12}$, IF protein is degraded to release free $B_{12}$).[16] The vitamin $B_{12}$-bearing nanoparticles would then be transported out of the lysosome, as $B_{12}$ is assumed to do by a yet unidentified mechanism.[17] Of key significance is that studies on the mechanism of cellular internalization and intracellular trafficking of $B_{12}$-conjugated nanoparticles have not been reported previously in the literature.

Our aim, therefore, was to probe the mechanisms of entry and transport across the cells of nanoparticles conjugated to vitamin $B_{12}$, and so demonstrate a model system that might have wider implications for delivery of therapeutic and/or diagnostic nanoparticles in general.[18–20] The model carrier was prepared from functionalized polystyrene (PS) nanoparticles spanning the 50–200 nm size range, covering viral dimensions and those reported optimal for endocytotic processes.[21] Nanoparticle surface decoration with the vitamin $B_{12}$ ligand was carried out by preparing an $\alpha$-$\omega$-aminohexylcarbamate derivative of $B_{12}$, which was then conjugated to carboxylated PS nanoparticles by standard carbodiimide chemistries. Cell studies were conducted using the Caco-2 (human intestinal) cell line cultured on permeable membrane supports, as a model of the intestinal epithelium that is most extensively used to study vitamin $B_{12}$-mediated drug delivery.[8,22,23] These cell cultures exhibit unidirectional transport of vitamin $B_{12}$ in the apical-to-basolateral direction,[8] and also in an IF-dependent and IF-independent fashion. The latter is attributed to the expression of the receptor transcobalamin II-R (responsible for the internalization of transcobalamin II in vivo) on the apical surface.[24] Initially the suitability of the Caco-2 cell culture model was verified by confirming the expression of cubilin receptor, as well as the presence and function of caveolae- and clathrin-mediated endocytic pathways.

We discovered that the vitamin $B_{12}$ ligand-mediated pathway was affected and perturbed by the attachment of vitamin $B_{12}$ to the nanoparticles. Vitamin $B_{12}$-nanoparticles bypassed the lysosomal compartments, with their cellular internalization and transport remaining largely unaffected by the inhibitors of clathrin-mediated endocytosis–the route governing vitamin $B_{12}$-IF internalization in vivo. Cell internalization and transport behavior of $B_{12}$-nanoparticles was instead markedly impeded by specific inhibitors of caveolae-mediated endocytosis, demonstrating that vitamin $B_{12}$-conjugated nanoparticles were trafficked by a different intracellular pathway to both free vitamin $B_{12}$ and unmodified nanoparticles. Overall, our study demonstrates that the attachment of ligands to nanoscale carriers can perturb the natural biological pathway of the ligand: a phenomenon that can be potentially exploited for delivery of biotherapeutics.

## 2. Results

### 2.1. Characterization and Conjugation of $\alpha$-$\omega$-Aminohexylcarbamate Vitamin $B_{12}$ to Functionalized Nanoparticles

The characterization and conjugation of amino-derivatized vitamin $B_{12}$ is shown in **Figure 1**. The 5′-hydroxyl group in the cyanocobalamin ribose ring was activated with 1,1′-carbonyldiimidazole (CDI) to be immediately derivatized with a slight excess of 1,6-hexanediamine (Figure 1A). Derivatization of cyanocobalamin was confirmed by means of nuclear magnetic resonance (NMR), mass spectrometry (MS), and high-performance liquid chromatography (HPLC) (Supporting Information, Figures S1-S5). Inspection of the $^1$H-NMR signals for the ribose ring revealed that these signals were significantly shifted after functionalization, especially those closer to the 5′ hydroxyl group. In addition, new signals arising from the C6 linker could be observed (Figure 1B and Supporting Information, Figure S1). The purity of the material was confirmed both by HPLC and MS, with the observed Mw of 1499.39 (Supporting Information, Figures S4 and S5, respectively).

The synthesized $\alpha$-$\omega$-aminohexylcarbamate vitamin $B_{12}$ derivative was reacted with carboxy functionalized, fluorescent (Yellow-Orange) PS nanoparticles in the presence of 1-ethyl-3-[3-dimethylaminopropyl]carbodiimide (EDAC) and *N*-hydroxy-succinimide (NHS) to yield, after purification by dialysis, the desired vitamin $B_{12}$-conjugated nanoparticles (Figure 1C).

The fluorescence quenching property of vitamin $B_{12}$[25,26] was used in order to confirm that conjugation of vitamin $B_{12}$ to nanoparticles had occurred (Supporting Information, Figure S6). The comparison of fluorescence intensities showed a markedly lower fluorescence for YO nanoparticles with surface conjugated vitamin $B_{12}$, relative to that of unmodified counterparts (Figure 1D and Supporting Information, Figure S6A). Presence of free vitamin $B_{12}$ in a suspension of unmodified YO nanoparticles also resulted in a decrease in nanoparticle fluorescence intensity with increasing amount of free vitamin $B_{12}$ (Supporting Information, Figure S6B), but the fluorescence was in this case restored after removal of free vitamin $B_{12}$ by dialysis (Supporting Information, Figure S6C). On the contrary, for vitamin $B_{12}$-conjugated nanoparticles, the fluorescence intensity was not reversed following dialysis (Supporting Information, Figure S6C), confirming that conjugation occurred.

  

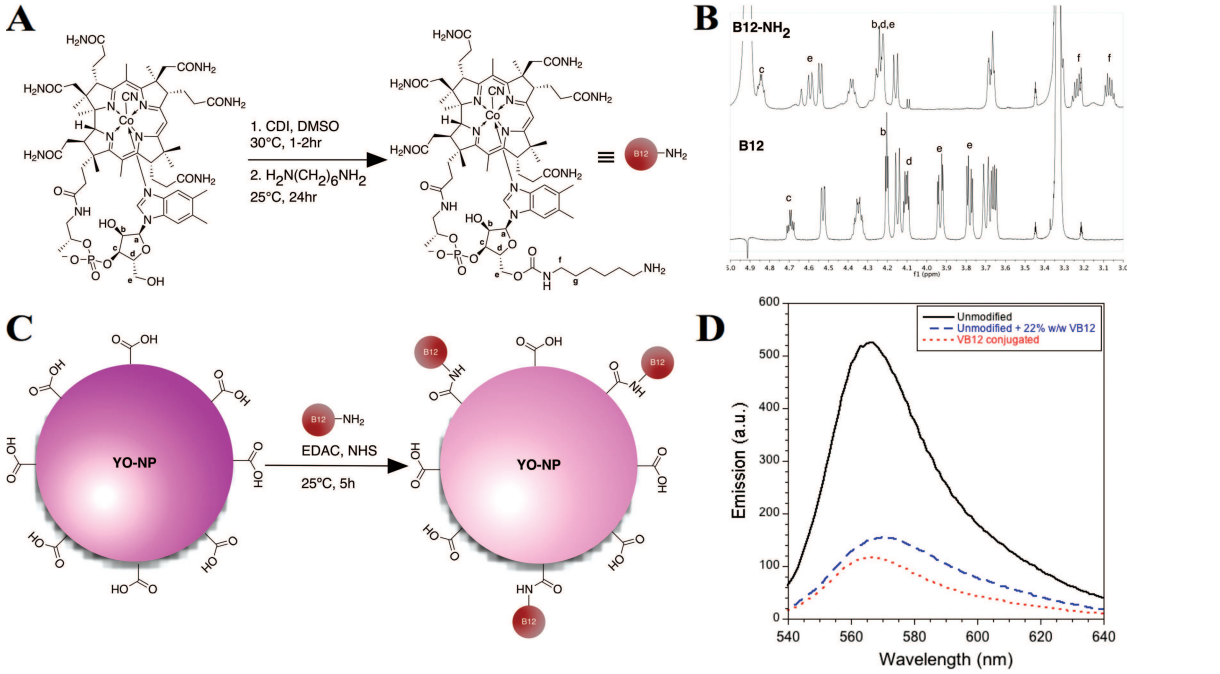


**Figure 1.** A) Synthesis of $\alpha$-$\omega$-aminohexylcarbamate-vitamin $B_{12}$ (schematic). B) $^1$H-NMR (expanded region) of purified vitamin $B_{12}$ (labelled 'B12') and $\alpha$-$\omega$-aminohexylcarbamate-vitamin $B_{12}$ (labelled 'B12-$NH_2$'). C) Schematics of the $\alpha$-$\omega$-aminohexylcarbamate-vitamin $B_{12}$ conjugation to fluorescent Yellow-Orange carboxylated polystyrene nanoparticles ('YO-NP'). D) Fluorescent spectra of YO (50 nm) unmodified nanoparticles ('Unmodified'), unmodified YO nanoparticles in the presence of vitamin $B_{12}$ in solution ('Unmodified + 22% w/w $VB_{12}$') and vitamin $B_{12}$-conjugated YO (50 nm) nanoparticles ('$VB_{12}$ conjugated'). Detailed characterization of both $\alpha$-$\omega$-aminohexylcarbamate-vitamin $B_{12}$ and $B_{12}$-conjugated nanoparticles is included in Supporting Information.

The vitamin $B_{12}$ quenching phenomenon was also exploited in an attempt to obtain quantitative information on the conjugation, by plotting the maximal emission peaks as a function of the weight percentage of free $B_{12}$ added (Supporting Information, Figure S6B) to an exponential decay model (Supporting Information, Figure S6D) ($R^2 \geq 0.997$). However, this resulted in an overestimation of $B_{12}$ attachment to nanoparticles, as the obtained values exceeded those theoretically possible for shoulder-to-shoulder conjugation. This may be due to differences in the fluorescence quenching effect of free and covalently bound vitamin $B_{12}$. In fact, a red shift in fluorescence was observed for the YO nanoparticles in the presence of free $B_{12}$, that was not detected in PS nanoparticles with covalently-bound $B_{12}$ (Figure 1D and Supporting Information, Figure S6), which would be due the dependence of a quenching effect on diffusion and the distance between the two species.[27]

The extent of $B_{12}$ conjugation to nanoparticle surface depends on the number of functional acid groups available. To investigate this, potentiometric titration experiments on unmodified nanoparticles (Supporting Information, Figure S7) estimated values for the number of carboxy groups per 1 $nm^2$ particle surface area to be 2.2 for 50 nm, 8.9 for 100 nm, and 20.8 for 200 nm nanoparticles. Although it was not possible to confirm this data with the nanoparticle manufacturer, the high surface density of acidic functional groups, also reported by others,[28] exceeds the number of ligand groups *per* $nm^2$ required for theoretical shoulder-to-shoulder conjugation of $B_{12}$, assuming a 4 $nm^2$ projected surface area for vitamin $B_{12}$. Therefore, it was reasoned that the level of $B_{12}$ conjugation to the nanoparticle surface would not be limited by the availability of acidic groups, but by the conjugation efficiency.

The conjugation reaction employed an excess (10 mg) of vitamin $B_{12}$ derivative for all nanoparticle sizes ('shoulder-to-shoulder' conjugation would require 1.85 mg, 0.92 mg, and 0.46 mg $B_{12}$ for 50, 100, and 200 nm nanoparticles, respectively). Considering that the conjugation efficiency is not expected to be significantly affected by nanoparticle size, and with an excess of both charged groups and vitamin $B_{12}$ derivative (compared to amount required for shoulder-to-shoulder conjugation), we would anticipate similar conjugation per surface area on the nanoparticles of all sizes, which would result in a similar spatial distribution of vitamin $B_{12}$ ligand on the surface of 50 nm, 100 nm, and 200 nm nanoparticles. Nanoparticle-bound ligand presentation to the cells would therefore be similar, assuming its statistical distribution on the nanoparticle surface, which is important considering that the ligand surface density plays a role in cellular interaction and uptake of nanoparticulates.[29–33]

Particle size analysis demonstrated an increased average hydrodynamic radii and broader size distribution profiles for conjugated, relative to unmodified, nanoparticles (Supporting Information, Figure S8). However, the observed average particle size falls within the size limits that could potentially affect the cell internalization behavior of nanoparticles.[21] It should be noted that all nanoparticles in this work are referred according to the size specified by the manufacturer; in the case of $B_{12}$-conjugated nanoparticles, this size is the pre-conjugation size. Vitamin $B_{12}$ conjugation was

NANO MICRO small

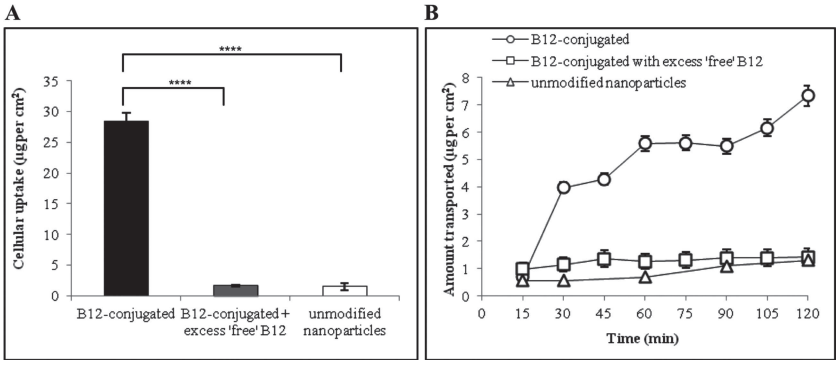


**Figure 2.** Cell uptake and transport of unmodified and vitamin $B_{12}$-conjugated nanoparticles in Caco-2 monolayers. A) Cell uptake of $B_{12}$-conjugated nanoparticles, alone or in the presence of excess 'free' vitamin $B_{12}$ (500 µg) in medium, and uptake of unmodified nanoparticles. B) Transport of $B_{12}$-conjugated nanoparticles across the cell monolayers, alone or in the presence of excess 'free' $B_{12}$, and transport of unmodified nanoparticles. Yellow-Orange PS nanoparticles of 50 nm nominal diameter were used. All experiments were conducted in the presence of intrinsic factor (IF). Data represents the mean ± SD (n = 3).

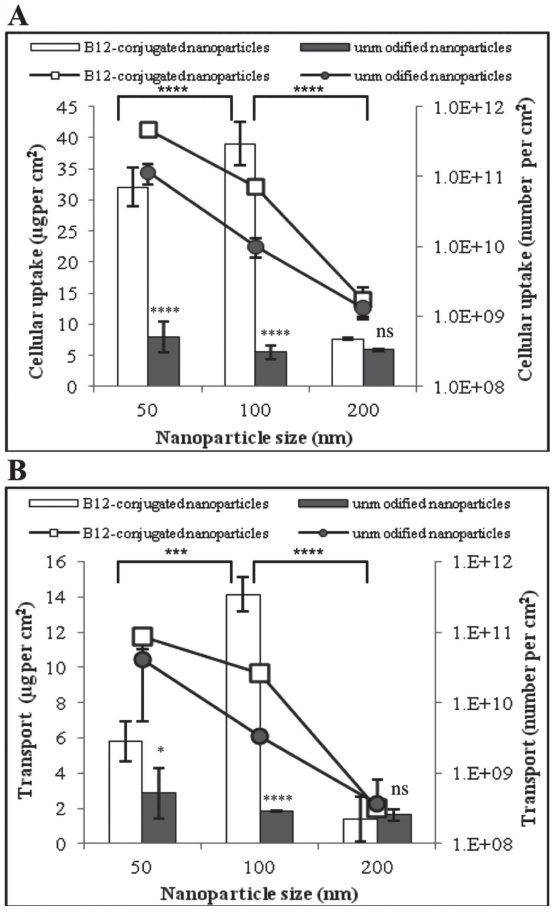


**Figure 3.** Effect of particle size on cell uptake and transport of vitamin $B_{12}$-conjugated nanoparticles in Caco-2 monolayers. A) Cell uptake expressed as mass (bar, left y-axis) and number (line, right y-axis) of nanoparticles per surface area of the cell monolayer. B) Transport across the cell monolayers expressed as mass (bar, left y-axis) and number of nanoparticles (line, right y-axis) per surface area of the cell monolayer. Data represents the mean ± SD (n = 3). Statistical analysis compared mass values for cell uptake and transport. Statistical comparisons indicated in the graphs: 100 nm vs 50 nm and 200 nm vs 100 nm for $B_{12}$-conjugated nanoparticles and $B_{12}$-conjugated vs unmodified nanoparticles of the same nominal size.

also indicated by a decrease in zeta potential values of the conjugated, relative to unconjugated nanoparticles (Supporting Information, Table S1). However, the decreased zeta potential values (measured in the biological solution in which the nanoparticles were applied to the cells) were sufficient to provide charge stabilization of the nanoparticle colloidal suspension.

### 2.2. Cell Uptake and Transport of Vitamin $B_{12}$-Conjugated Nanoparticles

Cell uptake studies (**Figure 2**A) demonstrate that internalization of 50 nm vitamin $B_{12}$-conjugated nanoparticles occurred to a markedly greater extent, amounting to 28 µg/cm$^2$ (nanoparticle amount per cell monolayer area) following a 3-h experiment, as compared to unmodified nanoparticles of the same size, which corresponded to 1.5 µg/cm$^2$. Furthermore, a competitive inhibition study reveals that the cellular uptake of vitamin $B_{12}$-conjugated nanoparticles was notably inhibited by the presence of excess soluble vitamin $B_{12}$, from 28 µg/cm$^2$ to 1.7 µg/cm$^2$ (Figure 2A), indicating vitamin $B_{12}$ receptor involvement in the process of cell uptake of vitamin $B_{12}$-conjugated nanoparticles. Regarding transcellular transport of nanoparticles, the experiments (Figure 2B) demonstrate a significantly increased translocation of $B_{12}$-conjugated nanoparticles across the cell monolayers, relative to the unmodified counterparts, with a level of transport of 7.3 µg/cm$^2$ and 1.3 µg/cm$^2$ (in a 2-hour experiment), respectively. The transcellular transport was reduced in the competitive experiment where $B_{12}$-conjugated nanoparticles were co-applied with excess free vitamin $B_{12}$ to 1.4 µg/cm$^2$.

### 2.3. Effect of Nanoparticle Size on Cell Uptake and Transport of Vitamin $B_{12}$-Conjugated Nanoparticles

In terms of the mass of nanoparticles, vitamin $B_{12}$-conjugation promoted a significant increase in cell internalization for 50 and 100 nm-sized nanoparticles, as compared to unmodified nanoparticles (**Figure 3**A), with the level of internalization of 39 µg/cm$^2$ for 100 nm and 32 µg/cm$^2$ for 50 nm nanoparticles. Cell uptake of $B_{12}$-conjugated nanoparticles of 200 nm (8 µg/cm$^2$) was, however, not statistically different to unmodified nanoparticles of the same size (6 µg/cm$^2$) (Figure 3A). Expressing the same data in terms of the number of nanoparticles, it is apparent that 50 nm $B_{12}$-conjugated nanoparticles were taken up by the cells in the greatest number ($4.7 \times 10^{11}$/cm$^2$), followed by 100 nm ($7.1 \times 10^{10}$) and 200 nm nanoparticles ($1.7 \times 10^9$).

Data showing transport of vitamin $B_{12}$-conjugated nanoparticles across the cell monolayers (Figure 3B) reveals that an increase in nanoparticle size from 50 to 100 nm resulted in an increased mass of translocated nanoparticles, from 5.8 µg to 14 µg. This is reduced to 1.4 µg

  

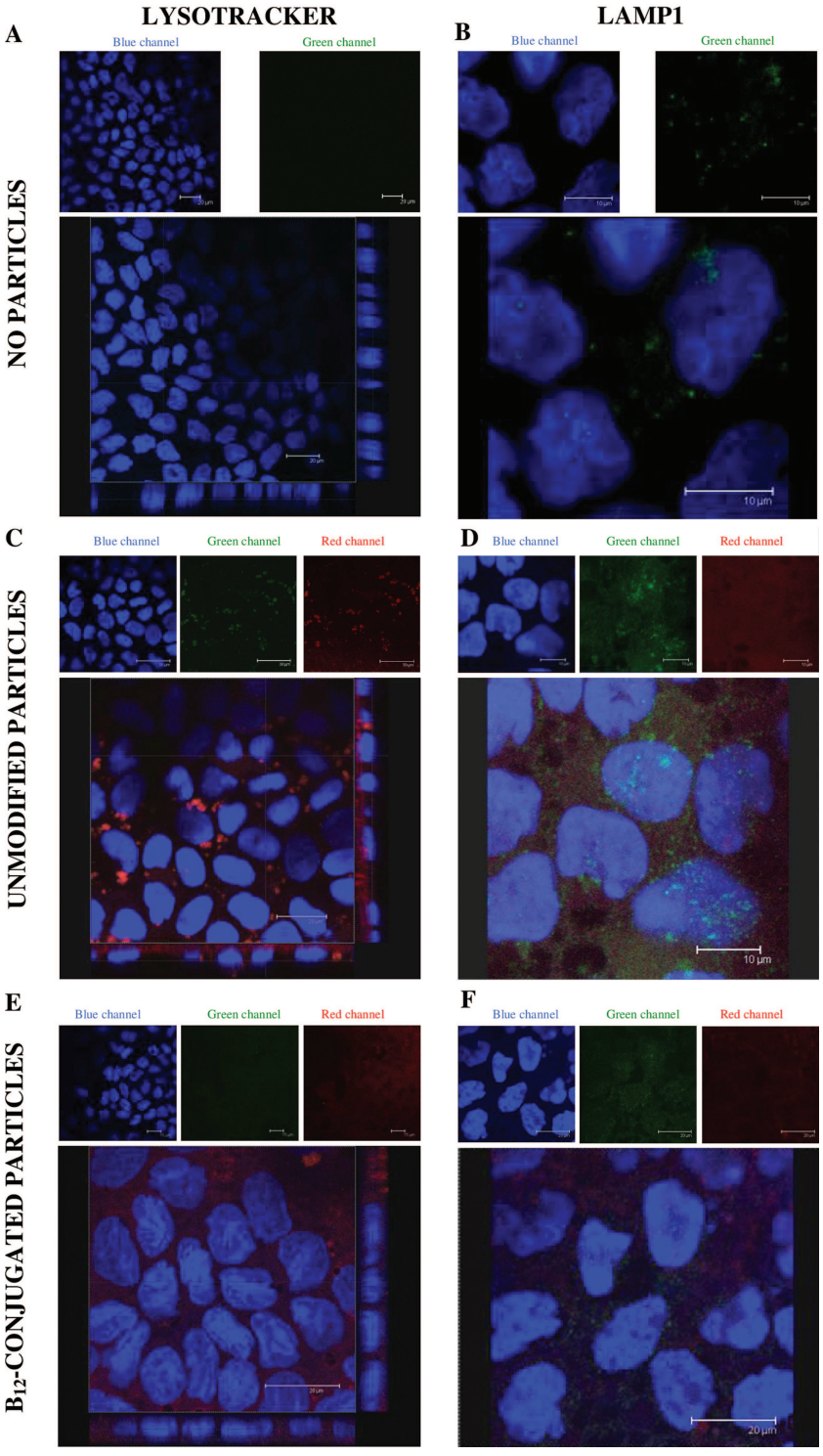


**Figure 4.** Confocal micrographs showing the uptake of $B_{12}$-conjugated nanoparticles (50 nm diameter) by Caco-2 monolayers. A) Cell staining with Lysotracker Green DND-26 in the absence of nanoparticles. B) Immunostaining for lysosomal associated-membrane protein 1 (LAMP1, green) in the absence of nanoparticles. C) Co-localisation of unmodified nanoparticles (red) with Lysotracker Green DND-26 (green), appearing as orange in some areas of the image. D) Immunostaining for LAMP1 protein (green) following cell incubation with unmodified nanoparticles (red). E) Staining with Lysotracker Green DND-26 (green) after cell incubation with vitamin $B_{12}$-conjugated nanoparticles (red). F) Immunostaining for LAMP1 (green) following exposure of cells to vitamin $B_{12}$-conjugated nanoparticles (red). Lysotracker Green DND-26 excitation 504 nm, emission 511 nm; YO nanoparticle excitation 529 nm, emission 546 nm; cell nuclei stained with Hoechst 33342 (blue). Scale bars indicated within individual images.

with a further increase in nanoparticle size to 200 nm. Considering the number of nanoparticles transported across the cell monolayers, there was a decrease from $8.5 \times 10^{10}$ to $2.6 \times 10^{10}$ to $3.2 \times 10^{8}$ as nanoparticle size increased from 50 nm to 100 nm and 200 nm, respectively, indicating a 3-fold reduction in transport when nanoparticle diameter increased from 50 to 100 nm, and a substantial 81-fold reduction in transport for the size increase from 100 to 200 nm.

### 2.4. Intracellular Localization of Vitamin $B_{12}$-Conjugated Nanoparticles

Two complementary techniques were employed, as shown in **Figure 4,** to assess whether $B_{12}$-conjugated nanoparticles reached the lysosomal compartment–the terminal destination of the IF-$B_{12}$ complex following its cell internalization. The Lysotracker probe was used to identify active lysosomal compartments,[34] whereas immunostaining for lysosomal associated membrane protein (LAMP1) was employed as a marker for a structural component of the lysosomes.[35,36] Since LAMP1 protein is ubiquitously expressed in the cells, anti-LAMP1 antibody was used in this case to identify localized or clustered protein regions, likely to be representative of lysosomal structures. Control confocal imaging experiments conducted on cell monolayers that were not exposed to nanoparticles illustrate the absence of Lysotracker green staining (Figure 4A), attributable to the existence of small, inactive primary lysosomes,[37] as well as the potential loss of staining during cell fixation.[38] Similarly, these control experiments also show a low level of LAMP1 immunostaining (Figure 4B).

Application of unmodified nanoparticles to Caco-2 monolayers resulted in their co-localization with the Lysotracker marker (Figure 4C). A series of control experiments ensured that the imaged pattern did not result from potential cross-emission between the YO fluorophore of nanoparticles and Lysotracker (Supporting Information, Figure S9). Importantly, cells incubated with unlabelled, unmodified nanoparticles (stained and imaged under the Lysotracker settings) displayed a similar punctate Lysotracker staining pattern (Supporting Information, Figure S9E) to cells imaged following

NANO MICRO small

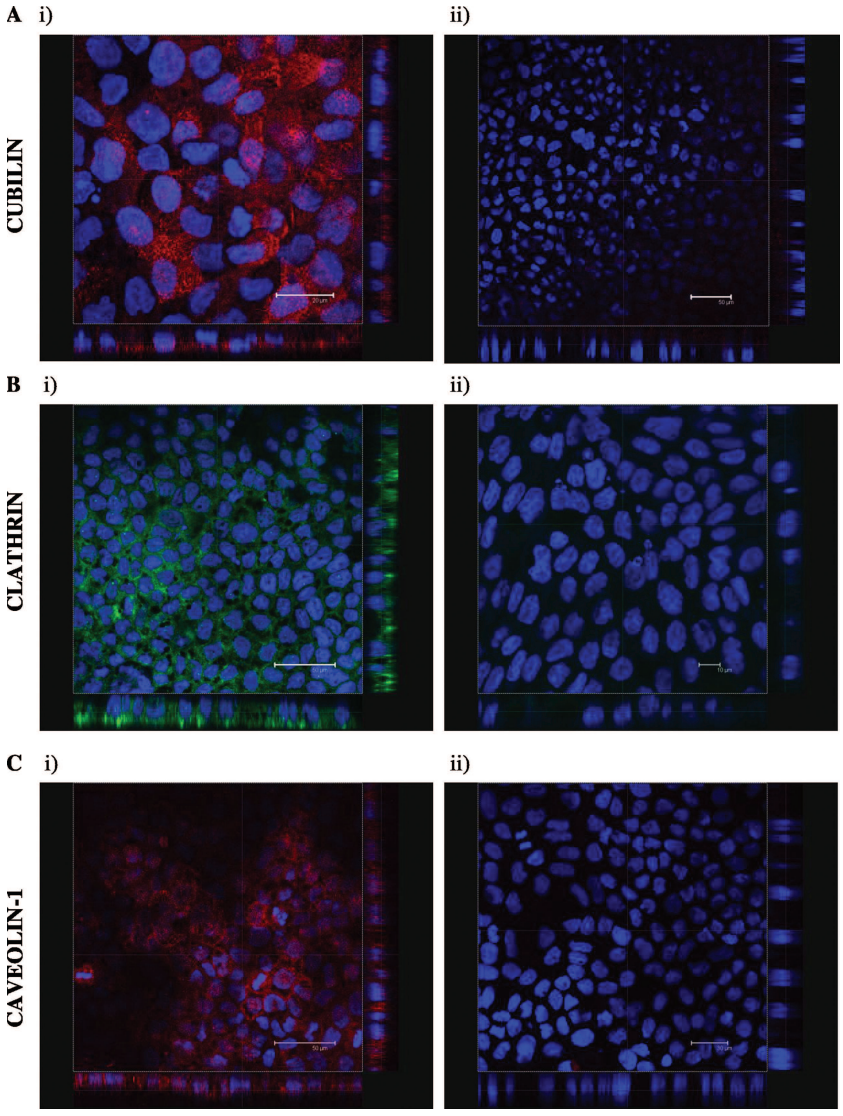


**Figure 5.** Immunostaining for cubilin receptor and selected endocytic components in Caco-2 cells, cultured as monolayers. A) i) Expression of cubilin receptor in cells treated with anti-human cubilin H300, followed by goat, anti-rabbit IgG-Rhodamine antibody (red) and ii) Control monolayer treated with the secondary, goat, anti-rabbit IgG-Rhodamine antibody only. B) i) Expression of clathrin, demonstrated by cell treatment with rabbit anti-clathrin primary antibody and goat, anti-rabbit IgG-FITC (green), and ii) Control monolayer treated with the secondary, goat, anti-rabbit IgG-FITC antibody only. C) i) Expression of caveolin-1, shown by treating cells with anti-human caveolin-1 H-97 antibody, followed by secondary goat, anti-rabbit IgG-Rhodamine antibody (red), and ii) Control monolayer, incubated with goat anti-rabbit IgG-Rhodamine antibody only. Cell nuclei were labelled with Hoechst 33342 (blue) in all cases. Immunostaining for all components was performed on day 21 of transwell culture.

application of unmodified YO (fluorescent) nanoparticles, indicating that this lysosomal probe is detectable in the presence of nanoparticles when larger lysosomal bodies are present (retaining the dye during cell fixation stage). Figure 4C, in conjunction with the control experiments in Figure S9, hence confirms the co-localisation of lysosomal Lysotracker stain and unmodified nanoparticles and that this is not an experimental artefact. On the contrary, following the application of vitamin $B_{12}$-conjugated nanoparticles to the cells, staining of lysosomal compartments with Lysotracker probe could not be observed (Figure 4E).

It should be noted that the potential buffering of lysosomes by internalized $B_{12}$-conjugated nanoparticles, and consequent absence of Lysotracker accumulation in acidic compartments, can be ruled out as the Lysotracker accumulation is clearly seen in Figure 4C when unmodified nanoparticles were applied and the presence of vitamin $B_{12}$ molecules does not afford buffering capability to the conjugated nanoparticles.

Regarding LAMP1 immunostaining, which is a marker for a lysosomal membrane protein, an indication of active lysosomes would be the formation of relatively larger structures, seen as globular regions following application of unmodified nanoparticles (Figure 4D), as opposed to a diffused fluorescence distribution pattern throughout the cytosol on application of $B_{12}$-conjugated nanoparticles (Figure 4F).

### 2.5. Cubilin Receptor, Caveolin-1, and Clathrin Expression in Caco-2 Cells

To validate the appropriateness of Caco-2 monolayers as a model to study the epithelial trafficking of vitamin $B_{12}$, the expression of the appropriate cellular components implicated in the vitamin $B_{12}$ pathway, including the vitamin $B_{12}$ cell surface receptor (cubilin), components of clathrin-coated pits (implicated in the internalization of the soluble $B_{12}$-IF complex) and caveolae (another possible route for material internalization), was confirmed (**Figure 5**). Confocal micrographs (Figure 5Ai) reveal positive fluorescence signal from cubilin receptor immunostaining, strongly suggesting expression of this protein in Caco-2 cells. The lack of fluorescence in the control experiment, where cell incubation with the primary antibody was omitted, rules out experimental artefacts that may result from non-specific antibody binding (Figure 5Aii). Cell monolayers also stained positively for the expression of clathrin, as a protein responsible for the formation of clathrin 'coated-pits' (Figure 5Bi and control experiment in 5Bii).

There are contradictory reports regarding the presence of caveolin-1 in Caco-2 cells and their ability to internalize material via caveolae-like domains.[39–42] Expression of caveolin-1 protein in cells is generally considered sufficient and necessary to drive the formation of morphologically identifiable caveolae.[43–45] Staining for caveolin-1 protein (Figure 5Ci and ii) clearly indicates its presence in the Caco-2 monolayers. It should be noted that cells were permeabilized

  

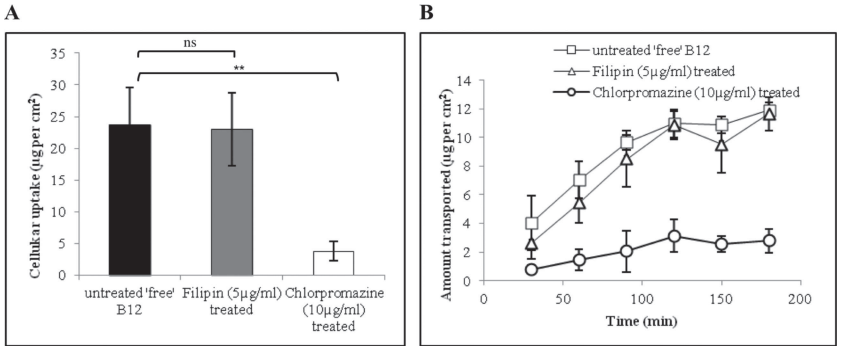


**Figure 6.** Effect of endocytic pathway-specific inhibitors on cell uptake and transport of soluble, 'free' vitamin $B_{12}$. A) Effect of chlorpromazine and filipin on cell uptake of vitamin $B_{12}$. B) Effect of chlorpromazine and filipin on transport of vitamin $B_{12}$ across Caco-2 monolayers. 'Untreated 'free' B12' denotes experiment in absence of inhibitors, 'Filipin (5 µg/mL) treated' denotes cell treatment with filipin, and 'Chlorpromazine (10 µg/mL) treated' denotes cell treatment with chlorpromazine. Vitamin $B_{12}$ was applied in presence of IF. Data represents the mean ± SD (n = 3).

prior to staining, in accordance with the generally accepted view that both the $NH_2$- and the COOH- termini of caveolin-1 face the cytoplasm and that no portion of the protein is extracellular.[46,47]

### 2.6. Cell Trafficking of Soluble Vitamin $B_{12}$

The previously documented cell uptake and transport mechanism of vitamin $B_{12}$-IF was confirmed initially by applying specific inhibitors of clathrin- and caveolae-mediated endocytosis. The uptake and transport-inhibiting effects of chlorpromazine (clathrin inhibition) and filipin (caveolae inhibition) in Caco-2 monolayers were initially validated by applying the pathway-selective ligands, transferrin[48,49] and cholera toxin B-subunit,[42,50] respectively (Supporting Information, Figure S10A–D). The internalization (**Figure 6**A) and transport (Figure 6B) of soluble vitamin $B_{12}$ were sensitive to the effects of chlorpromazine-mediated inhibition of the clathrin pathway (4-fold decrease) and were not significantly affected by the action of caveolae inhibitor, filipin. The data hence demonstrates that soluble vitamin $B_{12}$ (co-applied with IF) exploited a clathrin-mediated route in Caco-2 cells.

### 2.7. Cell Trafficking of Vitamin $B_{12}$-Conjugated Nanoparticles

Studies to decipher the cell trafficking pathways of vitamin $B_{12}$-conjugated nanoparticles initially employed chlorpromazine and filipin as pathway inhibitors, followed by additional experiments where clathrin- or caveolae-mediated pathways were inhibited by the way of potassium depletion[21,51] or genistein treatment,[52,53] respectively (**Figures 7** and **8**).

Chlorpromazine treatment did not produce a statistically significant reduction in the extent of cellular uptake of vitamin $B_{12}$-conjugated nanoparticles (Figure 7Ai). This is in contrast to the experiment shown in Figure 6A, which depicts a significant chlorpromazine-induced inhibition of cell internalization of soluble vitamin $B_{12}$ under comparable conditions. Considering the effect of chlorpromazine on the transport of vitamin $B_{12}$-conjugated nanoparticles across the cells, Figure 7Aii shows a steady state transport in chlorpromazine-treated cells compared to a rapid initial rate, followed by a later decrease in rate, in untreated cells. Consequently, the amount of vitamin $B_{12}$-conjugated nanoparticles transported across the cells at the 3-hour measurement point reached the value seen in untreated cells. It is not entirely clear why such an

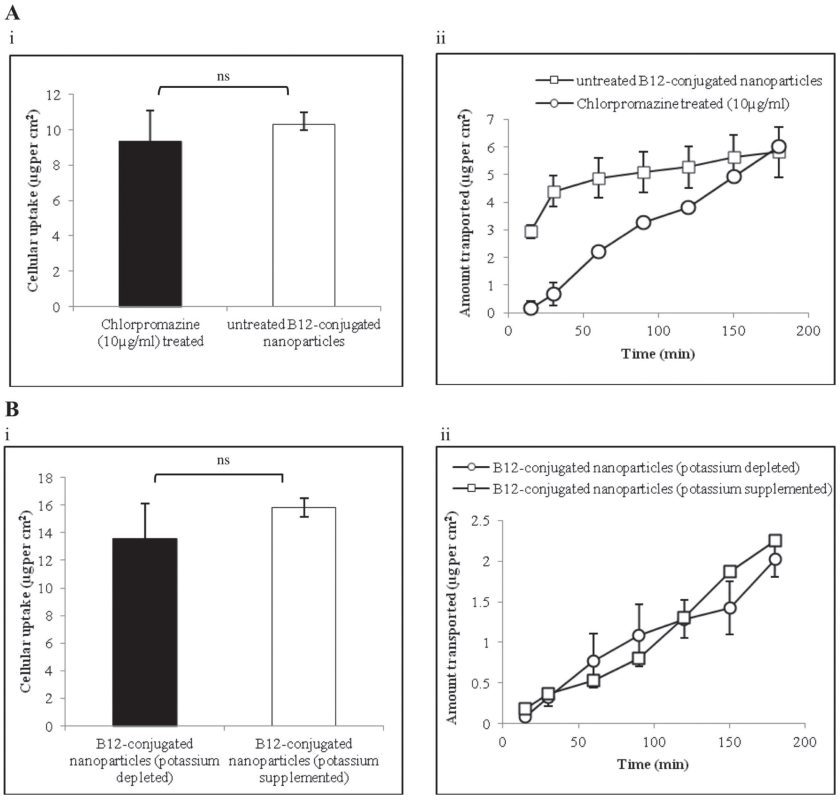


**Figure 7.** Effect of clathrin inhibition on cell uptake and transport of vitamin $B_{12}$-conjugated nanoparticles. A) Effect of chlorpromazine on (i) cell uptake and (ii) transport. B) Effect of potassium depletion on (i) cell uptake and (ii) transport. Studies were conducted with $B_{12}$-conjugated nanoparticles of 50 nm nominal diameter and in the presence of IF. 'Untreated B12-conjugated nanoparticles' denotes experiment in the absence of inhibitors, 'Chlorpromazine (10 µg/ml) treated' denotes cell treatment with chlorpromazine, 'B12-conjugated nanoparticles (potassium depleted)' denotes potassium depletion of cell medium and 'B12-conjugated nanoparticles (potassium supplemented)' denotes potassium supplementation of the medium. Data represents the mean ± SD (n = 3).

NANO MICRO small

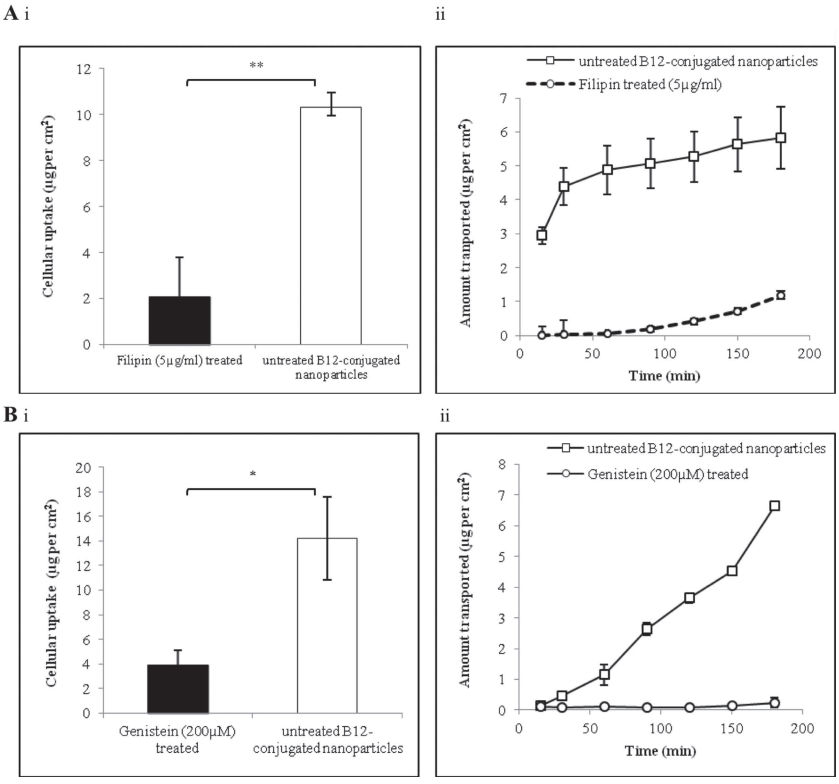


**Figure 8.** Effect of caveolae inhibition on the uptake and transport of vitamin $B_{12}$-conjugated nanoparticles. A) Effect of filipin on (i) cell uptake and (ii) transport of nanoparticles. B) Effect of genistein on (i) cell uptake and (ii) transport of nanoparticles. 50 nm vitamin $B_{12}$-conjugated nanoparticles applied in the presence of IF. 'Filipin (5 μg/mL) treated' denotes cell treatment with filipin, 'Untreated B12-conjugated nanoparticles' denotes experiment in absence of inhibitor and 'Genistein (200 μM) treated' denotes cell treatment with genistein. It should be noted that the control experiment depicting transport of $B_{12}$-conjugated nanoparticles across untreated cells, presented in Figure 7Aii, is also a control for this inhibition experiment. Data represents the mean ± SD (n = 3).

effect on transport was apparent, though it may have resulted from chlorpromazine interference with cytoskeletal function and consequent decreased transport of material towards the basolateral membrane.[54,55] It is important, however, that the curve profile in the Figure 7Aii is dramatically different the chlorpromazine inhibition seen in Figure 6B, indicating a clear difference of chlorpromazine effects on the transport of soluble vitamin $B_{12}$ and $B_{12}$-conjugated nanoparticles. In addition, the curve in Figure 7Aii is distinctly different to the profile in Figure S10B (Supporting Information) where transport of the pathway-selective ligand for clathrin (transferrin) is inhibited by the chlorpromazine-induced effect on clathrin-mediated pathway.

The data from experiments conducted in potassium-depleted medium again indicate no significant effect on cell uptake of vitamin $B_{12}$-conjugated nanoparticles when the clathrin pathway is inhibited, relative to the appropriate control (potassium supplemented medium) (Figure 7Bi). Likewise, potassium depletion did not affect the transport of $B_{12}$-conjugated nanoparticles relative to the unmodified control (Figure 7Bii). However, it must be noted that nanoparticle transport across the cell monolayers is markedly lower in the medium used in the potassium depletion experiments, even in the control experiment, compared to routinely used HBSS.

Treatment of cells by filipin (caveolae inhibitor) gave rise to a pronounced reduction in cell internalization of vitamin $B_{12}$-conjugated nanoparticles by approximately 5-fold (Figure 8Ai). The effect is mirrored in the significant inhibition of transport across the cell monolayers of vitamin $B_{12}$-nanoparticles in the presence of the same inhibitor (Figure 8Aii), whereby a level of transport of 5.8 μg in untreated cells was reduced to 1.2 μg in filipin-treated cell monolayers. Application of an alternative inhibitor specific for the caveolae endocytic pathway, genistein, again demonstrated a similar 5-fold reduction in cell uptake of vitamin $B_{12}$-conjugated nanoparticles (Figure 8Bi) and a dramatic suppression in their transport (Figure 8Bii).

Control experiments determining the uptake pathway of unmodified nanoparticles revealed that the inhibition of either clathrin or caveolae trafficking pathways did not produce a significant effect on the uptake and transport of non-functionalized 50 nm sized nanoparticles (Supporting Information, Figure S11).

## 3. Discussion

With recent developments in nano scale-based therapeutics there is a need to understand the processes of nanoparticulate interaction with the biological systems, including their trafficking by cells. An understanding of the biological pathways by which ligand-functionalized nanoparticle carriers engage whilst delivering their therapeutic payload is crucial for the development of such systems for a variety of clinical applications. The vitamin $B_{12}$ biological pathway has previously been considered for oral delivery of protein therapeutics and nanoparticle drug carriers. With respect to the latter, the cell trafficking mechanisms by which $B_{12}$-bearing nanosystems traverse the intestinal epithelium remain unstudied.

Here we investigated the trafficking of vitamin $B_{12}$-conjugated model (polystyrene) nanoparticle carrier in an intestinal epithelial cell model. To enable this, carboxy-functionalized, fluorescent nanoparticles were surface modified with the $\alpha$-$\omega$-aminohexylcarbamate vitamin $B_{12}$ derivative. Vitamin $B_{12}$ was amino derivatized using a 5′-ribose carbamate linkage, as such carbamate derivatives provide an increased affinity towards IF,[56] and the linkage is stable under the acidic conditions of the stomach.[56] Derivatization of cyanocobalamin was confirmed by NMR, MS and HPLC (Supporting Information, Figures S1–S5), whilst the fluorescence quenching property of vitamin $B_{12}$[25,26] was used to confirm $B_{12}$ conjugation (Supporting Information, Figure S6) following removal of 'free' vitamin $B_{12}$ by dialysis.

  

Vitamin $B_{12}$-conjugated nanoparticles exhibited a notably different behaviour, compared to unmodified nanoparticles, in terms of their cellular internalization and transport across the epithelial Caco-2 cell monolayers. Surface conjugation of $B_{12}$ significantly enhanced the uptake by and transport of nanoparticles across the polarized cells (Figures 2 and 3), whilst inhibition of these processes in the presence of excess soluble ('free') vitamin $B_{12}$ (Figure 2) suggests that the trafficking of $B_{12}$-conjugated nanoparticles in Caco-2 cells occurs through a vitamin $B_{12}$-mediated biological pathway.

Numerous published studies assessed the impact of particle size on their cellular uptake in vitro,[57,58] however rather fewer studies[8,59] have been conducted with systems where ligand-modified nanoparticles of specific size ranges were utilized to target epithelial transport pathways. This study employed vitamin $B_{12}$-conjugated 50, 100, and 200 nm PS lattices, encompassing the generally accepted size range for endocytosis in epithelial cells, to assess the biological mechanisms involved in the process of nanoparticle translocation across the Caco-2 epithelial barrier. Data was expressed in terms of nanoparticle mass (important from the drug delivery perspective), as well as nanoparticle number (potentially significant in understanding the number of events occurring). The data clearly demonstrates that, concerning the number of events occurring, an increase in nanoparticle size results in a decrease in the number of nanoparticles internalized, with this decrease being notably more prominent between 100 and 200 nm nanoparticles (41-fold), compared to that between 50 and 100 nm nanoparticles (approximately 7-fold). However, for mucosal delivery of therapeutics aiming to achieve a systemic effect, it would be desirable to obtain an absorption level that is sufficiently high to achieve a therapeutic effect. To this end, the amount of 14 μg/cm$^2$, which was found to traverse the cell monolayers in the case of 100 nm nanoparticles is significantly higher than that of 50 nm nanoparticles (5.8 μg/cm$^2$) and 200 nm systems (1.4 μg/cm$^2$). Additionally, vitamin $B_{12}$-conjugated nanoparticles of 50 and 200 nm were found to translocate across the cell monolayers less efficiently, with approximately 1 in 5.5 of internalized nanoparticles transported in both cases, relative to 100 nm nanoparticles where 1 in 2.8 of internalized nanoparticles crossed the cell monolayer barrier (Figure 4). One would therefore conclude that 100 nm nanoparticle systems could achieve optimal delivery capacities for a vitamin $B_{12}$-mediated oral delivery.

In the process of cell trafficking of soluble vitamin $B_{12}$ in vivo, the IF-$B_{12}$ complex is believed to be transported to the lysosome, where IF protein is degraded to release $B_{12}$.[16] From the perspective of transmucosal delivery of biologic drugs, this would mean that the $B_{12}$-modified nano-carrier (together with its active therapeutic) reaches the highly degradative lysosomal compartment, hence undermining its delivery potential. However, whether the intracellular trafficking of vitamin $B_{12}$-conjugated nano-carrier follows that same path has not been previously described in the literature. We hence employed $B_{12}$-conjugated 50 nm nanoparticles (particles of this size can enter the cells by different cell internalization pathways) and conducted a series of confocal (co-localization) and transport inhibition studies to decipher their intracellular trafficking. The data depicts that, unlike unmodified PS nanoparticles, vitamin $B_{12}$-conjugated counterparts did not co-localize with a marker for lysosomes (Figure 4), indicating that surface decoration of nanoparticles with vitamin $B_{12}$ gives rise to lysosomal bypass, hence suggesting a switch in cellular trafficking relative to both unmodified nanoparticles, as well as the route proposed for soluble vitamin $B_{12}$. The apparent weaker fluorescence intensity of vitamin $B_{12}$-conjugated nanoparticles compared to unmodified counterparts is a consequence of fluorescence quenching effect of vitamin $B_{12}$.

The cell trafficking pathway of soluble vitamin $B_{12}$ in vivo is relatively well established; $B_{12}$ initially binds to IF, followed by binding of $B_{12}$-IF complex to the cubilin receptor situated in the apical brush border membrane of the ileal mucosa.[60] Association of cubilin receptor with megalin, a member of the LDL receptor-related family of endocytic receptors,[61,62] leads to internalization of the entire cubilin receptor-IF-$B_{12}$ complex via clathrin-coated vesicles.[17] Our study initially confirmed the role of clathrin in the process of cell internalization of soluble vitamin $B_{12}$ (applied in combination with IF) in Caco-2 cells, as suggested by chlorpromazine-induced inhibition, while cellular transport remained largely unaffected by caveolae inhibitor, filipin (Figure 6).[21,42,50] In this experiment, both soluble vitamin $B_{12}$ and IF were used at a higher than physiological doses,[63] as the study was not designed to assess the absorption capacity of $B_{12}$ but to unravel the pathways involved in the process of epithelial transit. Similar levels of soluble vitamin $B_{12}$ transport across the Caco-2 monolayers obtained in this study (apparent permeability coefficient equivalent to $7.54 \times 10^{-7}$ cm/s) have also been reported in earlier studies employing comparatively high doses of vitamin $B_{12}$ in Caco-2 cells,[64,65] and may partly be contributed by passive paracellular transport, as suggested for other vitamin B family sub-types following high dose application.[66]

Experiments to elucidate the cell trafficking mechanism(s) of vitamin $B_{12}$-conjugated nanoparticles indicated that clathrin inhibition by chlorpromazine did not significantly affect the extent of their cell internalisation (as measured at 3 hours time point). However, considering the transport of $B_{12}$-conjugated nanoparticles across the cell layers in the presence of chlorpromazine, an inhibitory effect is present in the initial phase, relative to the control experiment, however the overall amount transported over the 3-hour experiment was not significantly affected (Figure 7A). The transport profile is dramatically different to a pathway selective ligand (Supporting Information, Figure S10B). Furthermore, cell uptake and transport of $B_{12}$-bearing nanoparticles was not affected in the potassium-depleted medium (Figure 7B), used as an alternative approach for clathrin pathway inhibition. This strengthens the suggestion, as derived from our data, that the clathrin pathway does not play a major role in trafficking of vitamin $B_{12}$-conjugated nanoparticles, although some involvement cannot be excluded. On the other hand, treatment with either filipin or genistein, as caveolae-inhibiting agents, resulted in a pronounced reduction in cellular internalization and transport of vitamin $B_{12}$-bearing nano-

  

NANO MICRO small

particles (Figure 8A and B). Interestingly, inhibition of either clathrin or caveolae trafficking pathways did not demonstrate a significant effect on the uptake and transport of unmodified nanoparticles, implying alternative (i.e. non-clathrin and non-caveolae) routes in their cell uptake and transport (Supporting Information, Figure S11). This further confirms that the involvement of the caveolar route is indeed specific to the $B_{12}$-conjugated nanoparticles.

The finding that vitamin $B_{12}$-bearing nanoparticles (in the presence of IF) predominantly exploit the caveolae-mediated route and evade lysosomes was not expected. The 'switch' in cell entry and intracellular trafficking could potentially result from the nature of vitamin $B_{12}$ ligand presentation to the cells. Presentation of multiple, particle-immobilised ligands in close proximity offers the possibility of a different interaction with IF and the cubilin receptor at the cell membrane, which following association with megalin receptor may trigger the caveolae rather than the clathrin pathway. Megalin receptor driven endocytosis has typically been associated with clathrin coated pits, although recent publications indicate the possibility of caveolae pathway involvement.[67,68]

## 4. Conclusion

We demonstrated that the surface-conjugation of vitamin $B_{12}$ to nanoparticles results in an unexpected intracellular trafficking behaviour in polarized epithelial cells, with a 'switch' in pathway: a finding that may have important implications for oral delivery of ligand-based nanoscale therapeutics and diagnostics. Considering that in the process of vitamin $B_{12}$ absorption in vivo, lysosomal function is essential for degradation of the associated IF,[17] further studies are necessary to ascertain whether vitamin $B_{12}$-conjugated nanoparticles retain IF on exit from the cells and if so, what are the consequences from a therapeutic perspective. However, the synergistic particle size and ligand decoration effects observed in epithelial cultures on the intracellular trafficking of $B_{12}$-conjugated nanoparticles is, to the best of our knowledge, a previously unreported example of controlled pathway switching in this way. These findings may provide significant new insights and chemical 'design rules' for nanoparticulate systems, which could enable their practical use in delivery of therapeutic and diagnostic macromolecules across the intestinal epithelium.

## 5. Experimental Section

Solid 1,1'-carbonyldiimidazole (CDI), anhydrous dimethyl sulfoxide, cyanocobalamin and *N*-hydroxy-succinimide (NHS) were purchased from Acros®. 1,6-hexanediamine, ethyl acetate and acetone were obtained from Fisher Scientific. 1-ethyl-3-[3-dimethylaminopropyl] carbodiimide (EDAC) was purchased from Calbiochem and all other chemicals and materials, unless otherwise stated, were purchased from Sigma-Aldrich or Fisher Scientific.

Thin layer chromatography (TLC) was conducted on silica gel $F_{254}$ from Fluka (Sigma-Aldrich) ($^{i}$PrOH 30 mL/*n*-BuOH 45 mL/$H_2O$ 21 mL/$NH_4OH$ 4 mL/TEA 1 mL). Mass spectra were recorded on a Waters ZMD spectrometer with a capillary voltage of 3.5 kV, a source temperature of 120 °C and a desolvation temperature of 350 °C.

Preparative high performance liquid chromatography (HPLC) of the product was carried out using a Waters and Associates system using a Waters X-Bridge C18 column (100 × 19 mm). The vitamin $B_{12}$ product was eluted with 100% water containing 10 mM ammonium formate and 0.1% (v/v) of ammonia solution (pH 9.5, solvent A) and 95% acetonitrile (Fisher Chemical, HPLC gradient grade) with 5% water and 0.1% ammonia solution (in water) (solvent B), using a gradient system at 20 mL/min comprising linear gradients from 3% to 10% v/v solvent B at 2 min, 35% v/v solvent B at 11.5 min and 95% v/v solvent B at 12 min. Purity (>95%) was determined using a Waters analytical HPLC system with a Waters 996 photodiode array detector at wavelengths 230–400 nm. NMR spectra of the product and starting material (cyanocobalamin) were obtained using a Bruker AV600 spectrometer equipped with a 5 mm TXI ($^{1}$H, $^{13}$C, $^{15}$N) cryoprobe running TopSpin v2.1 in deutero-methanol ($CD_3OD$) solution. This method was adapted from McEwan et al.[56]

### 5.1. Preparation of the $\alpha$-$\omega$-Aminohexylcarbamate Derivative of Cyanocobalamin

Solid CDI (260 mg, 0.32 mmol) was added to cyanocobalamin (1.0 g, 0.148 mmol) previously dissolved in anhydrous dimethyl sulfoxide (12 mL). The mixture was stirred for 1–2 h at 30 °C. Dry 1,6-hexanediamine (314 mg, 0.54 mmol) was added and the mixture stirred at room temperature over 24 h. The mixture was poured into ethyl acetate (30 mL) and left to stand. Following brief centrifugation, the supernatant was decanted and the residue sonicated for 5 min in acetone (50 mL). The resulting precipitate was filtered and the solid washed in acetone. The crude product was purified by silica column chromatography (45% v/v 2-propanol, 30% v/v n-butanol, 2% v/v ammonia and 25% v/v water) and then lyophilised.

### 5.2. Preparation of Vitamin $B_{12}$-Conjugated Nanoparticles

Fluorescent carboxylate Yellow Orange (YO, fluorescence spectra equivalent to rhodamine) polystyrene (PS) nanoparticles of 50 nm, 100 nm, and 200 nm (PolySciences Inc, 1 mL of 2.69, 2.6 and 2.63% w/v aqueous suspension, respectively) were modified with the $\alpha$-$\omega$-aminohexylcarbamate vitamin $B_{12}$ derivative (10 mg) by activation with 1-ethyl-3-[3-dimethylaminopropyl]carbodiimide (EDAC), in the presence of *N*-hydroxy-succinimide (NHS). The reaction was left to proceed for 5 h followed by incubation with glycine (100 mg/mL) in 50 mM carbonate buffer, pH 9.5, to block residual activated carboxyl sites. The particles were dialyzed extensively against distilled water over 24 h, with the water exchanged at regular intervals.

### 5.3. $B_{12}$-Conjugated Nanoparticle Characterization

The fluorescence quenching properties of vitamin $B_{12}$[25,26] were used to demonstrate the conjugation of the ligand on the surface of fluorescent carboxylated polystyrene (PS) nanoparticles following dialysis to remove free ligand (Supporting Information, Figure S6). Fluorescence spectra of both vitamin $B_{12}$-conjugated and unmodified nanoparticles (400 μg/mL) were recorded on a

  

Cary Eclipse fluorimeter ($\lambda_{ex}$ = 529 nm). The unmodified nanoparticle suspensions were titrated with increasing amounts of cyanocobalamin (in 2–8 μg steps), which in order to prevent dilution of nanoparticles upon titration, was applied dissolved in the nanoparticle suspension. Spectra were recorded after each addition and calibration curves were generated based on percent weight of vitamin $B_{12}$ to nanoparticles against fluorescence intensity and fitted to an exponential decay model.

The concentration of carboxyl groups on the nanoparticles was determined from potentiometric titration. Experiments were conducted with unmodified nanoparticles (50, 100, 200 nm), using a Fisher brand Hydrus 600 pH meter and a Thermo Fisher Orion 911 pH electrode at room temperature (23 °C). Unmodified nanoparticles were diluted 1:5 using distilled water. The pH of the nanoparticle suspensions was lowered to 1.70 using 1 M HCl. Stepwise additions of 0.1 M NaOH were made until neutral pH was attained. The concentration of carboxyl groups was calculated from the difference between the number of moles of HCl originally added and those of NaOH used for neutralisation. The density of the carboxylic acids on the surface ($d_a$) expressed in number per $nm^2$ was calculated using the equation:

$$d_a = \frac{mol_a \times N_A}{NP \times SA}$$

where $mol_a$ is the calculated mol of acid, $N_A$ is Avogadro's number, NP is the number of nanoparticles in sample (calculated from the density provided by the manufacturer and corrected for dilution) and SA is particle surface area, expressed in $nm^2$ (from manufacturer's specification).

The mean diameter and size distribution of nanoparticles (unmodified and vitamin $B_{12}$-conjugated) was determined by dynamic light scattering (DLS) using a Viscotek 802 system (Malvern Instruments). Size analysis was carried out on nanoparticles suspended in HBSS at pH 7.4 (biological buffer used in cell experiments). The results represent the mean of ten measurements at 25 °C. Nanoparticle zeta potential (suspended in HBSS, pH 7.4) was measured using a Zetasizer Nano ZS (Malvern Instruments).

### 5.4. Cell Culture

Caco-2 cells were obtained from the European Cell Culture Collection and used between passages 46–59. Cells were grown to confluence in 75 $cm^2$ flasks (canted neck and vented caps, Corning) in Eagle's Minimum Essential Medium (EMEM), supplemented with 10% foetal bovine serum, antibiotics and antimycotics, L-glutamine and non-essential amino acids. Upon confluence, cells were detached from the flasks and seeded on permeable supports (Transwell, Corning, 12 mm diameter, 1.1 $cm^2$, 0.4 μm pore size). Transepithelial Electrical Resistance (TEER, $\Omega cm^2$) was measured using a portable epithelial voltohmmeter (EVOM, World Precision Instruments) and cell monolayers with TEER exceeding 1000 $\Omega cm^2$ on day 21 of culture were deemed suitable for experiments.

### 5.5. Cell Uptake and Transport Studies

Culture medium was replaced with Hank's Balanced Salt Solution (HBSS), buffered with 2-[4-(2-hydroxyethyl)piperazin-1-yl]ethanesulfonic acid (HEPES, 20 mM) and cell monolayers incubated for 45 min. Unmodified YO nanoparticles (50, 100, 200 nm) and vitamin $B_{12}$-conjugated nanoparticles were suspended in HBSS/HEPES buffer to achieve a final nanoparticle concentration of 400 μg/mL. 3 μg of recombinant human intrinsic factor (rHUIF, Autogen Bioclear Ltd) was added per 1 mL of 400 μg/mL suspension of $B_{12}$-conjugated nanoparticles. This amounted to $7.13 \times 10^2$, $1.44 \times 10^3$ and $2.87 \times 10^3$ molecules of IF per 1 $\mu m^2$ surface area of 50, 100, and 200 nm nanoparticles, respectively. The solution was incubated at 37 °C prior to application to cells. Nanoparticle suspensions (0.5 mL) were applied to the apical chamber of triplicate wells and the Caco-2 cultures incubated at 37 °C over 3 h. At 30 min sampling intervals, 100 μL of the medium was removed from the basolateral side and fluorescence intensities were recorded. Sample losses were replaced with 100 μL of HEPES/HBSS. Cell uptake of nanoparticles was determined by measuring the supernatant fluorescence following cell lysis using 0.2% v/v Triton X-100 (Fluka) (10 min incubation) and centrifugation (to remove cell debris). Cell uptake and transport of nanoparticles was quantified by fluorescence (Dynex microplate reader, 529 nm/546 nm) using appropriate calibration curves for unmodified and conjugated nanoparticles.

The effect of soluble ligand competition on cell uptake of nanoparticles was assessed in the presence of excess cyanocobalamin (500 μg per 0.5 mL suspension of vitamin $B_{12}$-conjugated nanoparticles). Soluble vitamin $B_{12}$ transport studies were conducted in a similar manner to nanoparticle transport experiments, with vitamin $B_{12}$ applied to the cells at 1 mg/mL and quantified by UV absorbance (350 nm, Beckman Coulter DU 800 UV spectrophotometer).

### 5.6. Immunostaining for Cubilin Receptor, Clathrin and Caveolin-1

For immunostaining experiments, culture medium was removed and the cells (as polarized monolayers) fixed with 4% w/v paraformaldehyde (diluted in PBS) for 10 min at room temperature. For clathrin and caveolin-1 staining, an additional permeabilization step was conducted via the addition of 0.2% v/v Triton X-100 for 10 min. The cells were washed with PBS before incubation with 1% w/v BSA (in PBS; for 1 h). The primary antibodies for cubilin receptor and caveolin-1 (cubilin H-300; caveolin-1 H-97; rabbit, anti-human; Santa Cruz Biotechnology, Inc.) were diluted 1:50 with 1% BSA/PBS and incubated with the cells for 30 min. For clathrin immunostaining, the rabbit, anti-clathrin primary antibody (Abcam) was diluted 1:200 in 1% BSA/PBS. The cells were washed 3 times with PBS and incubated with the secondary antibody (goat, anti-rabbit IgG-rhodamine and goat, anti-rabbit IgG-FITC for cubilin/caveolin-1 and clathrin, respectively) diluted 1:100 (in 1% BSA/PBS) for another 30 min. The control cell layers were incubated with the appropriate secondary antibody only. Following a final wash step, the cell nuclei were stained with Hoechst 33342 (0.1 mg/mL), the cells washed and the filter membrane excised from the insert. Cells were mounted on a slide using 1,4-diazabicyclo[2.2.2]octane (DABCO) (1% diluted in 9:1 glycerol:PBS) and covered with a glass cover slip. Confocal images were taken using a Leica SP2 CLSM-Micro4 confocal microscope.

NANO MICRO small

### 5.7. Imaging of Nanoparticle Uptake and Lysosomal Staining

Caco-2 cells were cultured as polarized monolayers in the manner described above. Lysotracker Green DND-26 (Invitrogen) was diluted according to the manufacturer's instructions in HBSS and nanoparticles (unmodified or $B_{12}$-conjugated) were suspended in this solution to achieve a final nanoparticle concentration of 250 μg/mL. The suspension was incubated with IF prior to application to the cell, as described above. Lysotracker-containing nanoparticle suspension (0.5 mL) was applied to the apical side of the cell monolayers and cells incubated at 37 °C for 2 h. For anti-LAMP1 (lysosomal-associated membrane protein 1) immunostaining studies, nanoparticles (unmodified or $B_{12}$-conjugated) were applied (in HEPES-buffered HBSS) to the apical side and the cells incubated at 37 °C over 2 h. Following removal of the nanoparticle suspension and cell monolayer washing, the cells were then fixed with 4% paraformaldehyde. Cells were then permeabilized with 0.2% Triton X-100 over 10 min and after another wash step, incubated in 1% BSA/PBS at 4 °C for 1 h before the addition of anti-LAMP1 antibody (Sigma-Aldrich), diluted 1:50 in 1% BSA/PBS for 30 min. The cells were washed with PBS and incubated with the secondary antibody [goat, anti-rabbit IgG-FITC (Sigma-Aldrich)] diluted 1:100 (in 1% BSA/PBS) for another 30 min (whilst protecting from light). Following a final wash step, cells were stained for nuclei, followed by sample mounting on glass slides. Sample imaging was conducted by confocal microscopy, as detailed above.

Confocal imaging was conducted using a sequential scanning mode, where cross-emission between different fluorophores is minimized. However, a control set of experiments were conducted to verify that the imaged pattern did not result from fluorophore cross-emission between the Lysotracker marker and fluorescent nanoparticles. In these experiments, cell samples incubated with the Lysotracker probe were imaged using YO nanoparticle scan settings (529 nm/546 nm, excitation/emission), whilst cells treated with YO nanoparticles were visualized using Lysotracker scan settings (504 nm/511 nm excitation/emission) (Supporting Information, Figure S9).

### 5.8. Clathrin and Caveolae Inhibition Studies

Caco-2 cell monolayers were treated with inhibitors of specific endocytic pathways, genistein (200 μM), filipin (5 μg/mL) or chlorpromazine (10 μg/mL), diluted in HBSS/HEPES for 1 h at 37 °C prior to the addition of nanoparticles.[21] Unmodified and vitamin $B_{12}$-conjugated nanoparticles (in the presence of IF) were applied to the cells suspended in HBSS/HEPES (400 μg/mL) containing one of the above inhibitors for 3 h. At 30 min intervals, 100 μL samples were removed from the basolateral side for fluorescence determination in order to quantify nanoparticle transport across the cell monolayers. At the final sampling time point, nanoparticle internalization was determined following cell lysis, as described above. For the potassium depletion study, conducted to perturb clathrin-mediated endocytosis,[21,69] Caco-2 cells were washed once with potassium-free buffer (pH 7.4), containing 140 mM NaCl (BDH, Analar), 20 mM HEPES, 1 mM $CaCl_2$, 1 mM $MgCl_2$ and 1 mg/mL D-glucose (GIBCO), followed by a wash with a hypotonic buffer (potassium free buffer diluted 1:1 with water). The cells were then washed again twice with potassium free buffer. Control wells were treated with buffer (pH 7.4), containing 140 mM NaCl, 20 mM HEPES, 1 mM $CaCl_2$, 1 mM $MgCl_2$, 1 mg/mL D-glucose and 10 mM KCl. Vitamin $B_{12}$-conjugated nanoparticles were incubated with the cells in potassium-free or potassium-containing buffer as indicated. Subsequently, nanoparticle uptake and transport was determined by fluorescence.

As a control for clathrin-mediated uptake,[21] FITC-transferrin (Autogen Bioclear LTD, diluted in HBSS to a final incubation concentration of 100 μg/mL) was applied to the apical chambers in the presence or absence of chlorpromazine (10 μg/mL), a specific inhibitor of clathrin-mediated endocytosis. In addition, native cyanocobalamin (vitamin $B_{12}$) was also applied in the presence of IF and in conjunction with the same inhibitor, to confirm the route of internalization of the soluble ligand and cell uptake and transport was determined via UV-absorbance at 350 nm. To assess the specificity of filipin as an inhibitor of caveolae-mediated uptake,[40,70] transport of Alexa Fluor 488-labelled cholera toxin subunit B (Invitrogen, applied at 5 μg/mL) was determined following its application with or without filipin (5 μg/mL) (Supporting Information, Figure S10).

### 5.9. Statistical Analysis

All experiments were carried out using triplicate samples. One way analysis of variance (ANOVA) followed by Bonferroni post-hoc test was applied for comparison of group means of three or more groups, whilst Student's t-test was used for comparison of two groups. P values of <0.05 were considered statistically significant. *, **, *** and **** indicate $p < 0.05$, $p < 0.01$, $p < 0.001$ and $p < 0.0001$, respectively, whilst 'ns' indicates non-significant.

## *Supporting Information*

*Supporting Information is available from the Wiley Online Library or from the author. It includes characterization of the vitamin $B_{12}$ derivative (by means of NMR, MS and HPLC), fluorescence quenching experiments showing $B_{12}$-conjugation to nanoparticle surface, particle potentiometric titration experiments, nanoparticle size and zeta potential analyses, confocal cross-emission control experiments, cellular uptake and transport of FITC-transferrin and cholera toxin B-subunit and unmodified nanoparticles in the presence of clathrin- and caveolae-specific inhibitors.*

## *Acknowledgements*

*This work was funded by a BBSRC Industrial CASE grant with UCB Pharma*

[1] W. R. Algar, D. E. Prasuhn, M. H. Stewart, T. L. Jennings, J. B. Blanco-Canosa, P. E. Dawson, I. L. Medintz, *Bioconjugate Chem.* **2011**, *22*, 825–858.
[2] W. Gao, J. M. Chan, O. C. Farokhzad, *Mol. Pharmaceut.* **2010**, *7*, 1913–1920.
[3] Y. Yan, G. K. Such, A. P. R. Johnston, H. Lomas, F. Caruso, *ACS Nano* **2011**, *5*, 4252–4257.

  

[4] X. Zhang, K. K. Sharma, M. Boeglin, J. Ogier, D. Mainard, J. C. Voegel, Y. Mely, N. Benkirane-Jessel, *Nano Lett.* **2008**, *8*, 2432–2436.
[5] P. Ghosh, X. C. Yang, R. Arvizo, Z. J. Zhu, S. S. Agasti, Z. H. Mo, V. M. Rotello, *J. Am. Chem. Soc.* **2010**, *132*, 2642–2645.
[6] C. Tekle, B. van Deurs, K. Sandvig, T. G. Iversen, *Nano Lett.* **2008**, *8*, 1858–1865.
[7] G. J. Russell-Jones, in *Peptide-based Drug Design: Controlling Transport and Metabolism* (Eds: M. Taylor, G. Amidon), ACS Publications, USA **1995**, pp.181–198.
[8] G. J. Russell-Jones, L. Arthur, H. Walker, *Int. J. Pharm.* **1999**, *179*, 247–255.
[9] K. B. Chalasani, P. V. Diwan, K. P. Raghavan, S. K. Jain, K. K. Rao, G. J. Russell-Jones, 2002, US patent number 6482413.
[10] K. B. Chalasani, G. J. Russell-Jones, A. K. Jain, P. V. Diwan, S. K. Jain, *J. Control. Release* **2007**, *122*, 141–150.
[11] P. W. Swaan, *Pharm. Res.* **1998**, *15*, 826–834.
[12] G. J. Russell-Jones, S. W. Westwood, A. D. Habberfield, *Bioconjug. Chem.* **1995**, *6*, 459–465.
[13] K. B. Chalasani, G. J. Russell-Jones, S. K. Yandrapu, P. V. Diwan, S. K. Jain, *J. Control. Release* **2007**, *117*, 421–429.
[14] S. K. Moestrup, H. Birn, P. B. Fischer, C. M. Petersen, P. J. Verroust, R. B. Sim, E. I. Christensen, E. Nexo, *Proc. Natl. Acad. Sci. USA* **1996**, *93*, 8612–8617.
[15] E. I. Christensen, H. Birn, *Nat. Rev. Mol. Cell Biol.* **2002**, *3*, 256–266.
[16] M. M. Gordon, T. Howard, M. J. Becich, D. H. Alpers, *Am. J. Physiol.* **1995**, *268*, G33–40.
[17] P. L. Tuma, A. L. Hubbard, *Physiol. Rev.* **2003**, *83*, 871–932.
[18] Z. Krpetic, S. Saleemi, I. A. Prior, V. See, R. Qureshi, M. Brust, *ACS Nano* **2011**, *5*, 5195–5201.
[19] P. Nativo, I. A. Prior, M. Brust, *ACS Nano* **2008**, *2*, 1639–1644.
[20] W. H. De Jong, W. I. Hagens, P. Krystek, M. C. Burger, A. J. A. M. Sips, R. E. Geertsma, *Biomaterials* **2008**, *29*, 1912–1919.
[21] J. Rejman, V. Oberle, I. S. Zuhorn, D. Hoekstra, *Biochem. J.* **2004**, *377*, 159–169.
[22] C. J. Dix, I. F. Hassan, H. Y. Obray, R. Shah, G. Wilson, *Gastroenterology* **1990**, *98*, 1272–1279.
[23] N. Dan, D. F. Cutler, *J. Biol. Chem.* **1994**, *269*, 18849–18855.
[24] S. Bose, S. Seetharam, N. M. Dahms, B. Seetharam, *J. Biol. Chem.* **1997**, *272*, 3538–3543.
[25] J. Sun, X. Zhu, M. Wu, *J. Fluoresc.* **2007**, *17*, 265–270.
[26] H. Xu, Y. Li, C. Liu, Q. Wu, Y. Zhao, L. Lu, H. Tang, *Talanta* **2008**, *77*, 176–181.
[27] B. Valeur, *Molecular Fluorescence: Principles and Applications*, Wiley-VCH., Weinheim, Germany **2001**.
[28] J. S. Ahn, P. T. Hammond, M. F. Rubner, L. Ilsoon, *Colloids Surf., A* **2005**, *259*, 45–53.
[29] F. Gu, L. Zhang, B. A. Teply, N. Mann, A. Wang, A. F. Radovic-Moreno, R. Langer, O. C. Farokhzad, *Proc. Natl. Acad. Sci. USA* **2008**, *105*, 2586–2591.
[30] G. F. Dawson, G. W. Halbert, *Pharm. Res.* **2000**, *17*, 1420–1425.
[31] M. O. Oyewumi, R. J. Mumper, *Int. J. Pharm.* **2003**, *251*, 85–97.
[32] A. O. Saeed, J. P. Magnusson, E. Moradi, M. Soliman, W. Wang, S. Stolnik, K. J. Thurecht, S. M. Howdle, C. Alexander, *Bioconjug. Chem.* **2011**, *22*, 156–168.
[33] E. Moradi, D. Vllasaliu, M. Garnett, F. Falcone, S. Stolnik, *RSC Adv.* **2012**, *2*, 3025–3033.
[34] Molecular Probes product data sheet, probes.invitrogen.com/media/pis/mp07525.pdf, accessed: November, 2011.
[35] J. W. Chen, Y. Cha, K. U. Yuksel, R. W. Gracy, J. T. August, *J. Biol. Chem.* **1988**, *263*, 8754–8758.
[36] B. L. Granger, S. A. Green, C. A. Gabel, C. L. Howe, I. Mellman, A. Helenius, *J. Biol. Chem.* **1990**, *265*, 12036–12043.
[37] D. W. Fawcett. *The Cell*, W. B. Saunders Company, USA, Pennsylvania **1981**, pp.487–488.
[38] The Molecular Probes Handbook, http:/www.invitrogen.com/site/us/en/home/References/Molecular-Probes-The-Handbook/Probes-for-Organelles/Probes-for-Lysosomes-Peroxisomes-and-Yeast-Vacuoles.html, accessed December, 2012.
[39] N. Ullrich, A. Caplanusi, B. Brone, D. Hermans, E. Lariviere, B. Nilius, W. Van Driessche, J. Eggermont, *Am. J. Physiol. Cell Physiol.* **2006**, *290*, C1287–1296.
[40] J. M. Patlolla, M. V. Swamy, J. Raju, C. V. Rao, *Oncol. Rep.* **2004**, *11*, 957–963.
[41] F. J. Field, E. Born, S. Murthy, S. N. Mathur, *J. Lipid Res.* **1998**, *39*, 1938–1950.
[42] P. A. Orlandi, P. H. Fishman, *J. Cell Biol.* **1998**, *141*, 905–915.
[43] A. W. Cohen, R. Hnasko, W. Schubert, M. P. Lisanti, *Physiol. Rev.* **2004**, *84*, 1341–1379.
[44] S. Li, K. S. Song, S. S. Koh, A. Kikuchi, M. P. Lisanti, *J. Biol. Chem.* **1996**, *271*, 28647–28654.
[45] B. Razani, T. P. Combs, X. B. Wang, P. G. Frank, D. S. Park, R. G. Russell, M. Li, B. Tang, L. A. Jelicks, P. E. Scherer, M. P. Lisanti, *J. Biol. Chem.* **2002**, *277*, 8635–8647.
[46] P. Dupree, R. G. Parton, G. Raposo, T. V. Kurzchalia, K. Simons, *EMBO J.* **1993**, *12*, 1597–1605.
[47] M. Sargiacomo, P. E. Scherer, Z. Tang, E. Kubler, K. S. Song, M. C. Sanders, M. P. Lisanti, *Proc. Natl. Acad. Sci. USA* **1995**, *92*, 9407–9411.
[48] A. Motley, N. A. Bright, M. N. Seaman, M. S. Robinson, *J. Cell Biol.* **2003**, *162*, 909–918.
[49] M. Lakadamyali, M. J. Rust, X. Zhuang, *Cell* **2006**, *124*, 997–1009.
[50] J. E. Schnitzer, P. Oh, E. Pinney, J. Allard, *J. Cell Biol.* **1994**, *127*, 1217–1232.
[51] J. M. Larkin, M. S. Brown, J. L. Goldstein, R. G. Anderson, *Cell* **1983**, *33*, 273–285.
[52] M. A. van der Aa, U. S. Huth, S. Y. Hafele, R. Schubert, R. S. Oosting, E. Mastrobattista, W. E. Hennink, R. Peschka-Suss, G. A. Koning, D. J. Crommelin, *Pharm. Res.* **2007**, *24*, 1590–1598.
[53] R. G. Parton, B. Joggerst, K. Simons, *J. Cell Biol.* **1994**, *127*, 1199–1215.
[54] S. Mentzel, H. B. Dijkman, J. P. van Son, J. F. Wetzels, K. J. Assmann, *J. Histochem. Cytochem.* **1999**, *47*, 871–880.
[55] A. Wells, M. F. Ware, F. D. Allen, D. A. Lauffenburger, *Cell Motil. Cytoskel.* **1999**, *44*, 227–233.
[56] J. F. McEwan, H. S. Veitch, G. J. Russell-Jones, *Bioconjug. Chem.* **1999**, *10*, 1131–1136.
[57] O. Harush-Frenkel, N. Debotton, S. Benita, Y. Altschuler, *Biochem. Biophys. Res. Commun.* **2007**, *353*, 26–32.
[58] M. G. Qaddoumi, H. Ueda, J. Yang, J. Davda, V. Labhasetwar, V. H. Lee, *Pharm. Res.* **2004**, *21*, 641–648.
[59] G. J. Russell-Jones, H. Veitch, L. Arthur, *Int. J. Pharm.* **1999**, *190*, 165–174.
[60] B. Seetharam, D. H. Alpers, R. H. Allen, *J. Biol. Chem.* **1981**, *256*, 3785–3790.
[61] J. Gliemann, *Biol. Chem.* **1998**, *379*, 951–964.
[62] T. E. Willnow, *J. Mol. Med.* **1999**, *77*, 306–315.
[63] S. N. Fedosov, N. U. Fedosova, L. Berglund, S. K. Moestrup, E. Nexo, T. E. Petersen, *Biochemistry* **2005**, *44*, 3604–3614.
[64] F. Sarti, J. Iqbal, C. Muller, G. Shahnaz, D. Rahmat, A. Bernkop-Schnurch, *Anal. Biochem.* **2012**, *420*, 13–19.
[65] A. Tronde, B. Norden, H. Marchner, A. K. Wendel, H. Lennernas, U. H. Bengtsson, *J. Pharm. Sci.* **2003**, *92*, 1216–1233.
[66] M. Zielinska-Dawidziak, K. Grajek, A. Olejnik, K. Czaczyk, W. Grajek, *J. Nutr. Sci. Vitaminol.* **2008**, *54*, 423–429.
[67] A. Bento-Abreu, A. Velasco, E. Polo-Hernandez, C. Lillo, R. Kozyraki, A. Tabernero, J. M. Medina, *J. Neurochem.* **2009**, *111*, 49–60.
[68] A. Tanimura, F. Yamada, A. Saito, *J. Med. Invest.* **2011**, *58*, 140–147.
[69] I. S. Zuhorn, R. Kalicharan, D. Hoekstra, *J. Biol. Chem.* **2002**, *277*, 18021–18028.
[70] W. I. Lencer, T. R. Hirst, R. K. Holmes, *Biochim. Biophys. Acta* **1999**, *1450*, 177–190.

Received: October 23, 2012
Revised: February 5, 2013
Published online: May 2, 2013